

Absolute Raman-scattering cross section of a surface-adsorbed layer: Amorphous nitrobenzene on Ni(111)

K. Sakamoto, G. Mizutani,* and S. Ushioda

Research Institute of Electrical Communication, Tohoku University, 2-1-1 Katahira Aoba-ku, Sendai 980, Japan

(Received 1 April 1993)

We have determined the absolute Raman-scattering cross section of the NO_2 symmetric stretching mode (1346 cm^{-1}) of an amorphous nitrobenzene layer adsorbed on Ni(111). The layer thickness ranged from several monolayers to several hundred Å. The cross section was obtained by fitting the coverage dependence of the absolute Raman intensity to a theoretical curve where the electromagnetic Green's function for a multilayered geometry was used to account for the influence of the metallic substrate on the local incident electric field at the molecular site, and on the propagation of the scattered light. The molecules in the amorphous layer are assumed to be randomly oriented. The absolute differential Raman cross section and the depolarization ratio are $3.7 \times 10^{-28} \text{ cm}^2/(\text{molecule sr line plane of polarization})$ and 0.17, respectively. (This unit refers to the integrated intensity over the entire line width.) We verified that this cross section correctly predicts the Raman intensity for another arbitrary experimental geometry. We have also determined the absolute Raman-scattering cross sections for gaseous and liquid nitrobenzene. The ratios between these cross sections are gas:liquid:amorphous = 1:7:29. Part of this change in the measured Raman cross section for different phases can be explained by the difference in the local microscopic field.

I. INTRODUCTION

Although Raman-scattering spectroscopy is used extensively in studies of materials of all phases, the absolute scattering cross section is rarely measured in most of the work reported in the literature. This is due to the difficulty of determining this quantity with precision, particularly when the scattered light intensity is very weak. Another reason may be that even when an absolute cross section is obtained, there is usually no theoretical calculation with which to compare it. However, very important information is contained in the absolute cross section, particularly concerning the interaction of the scattering entity with its environment as in the case of surface-adsorbed molecules and ultrathin layers. As we show in this paper, the absolute cross section, especially its change with environment, can provide crucial information on the microscopic environment that surrounds the scattering molecule.

Surface Raman spectroscopy (SRS) has many advantages compared with other surface vibrational spectroscopies such as electron-energy-loss spectroscopy and infrared-absorption spectroscopy, and we have used SRS in vibrational studies of some adsorbate systems.¹⁻⁴ However, the measurements are difficult because of the extremely weak scattered light intensity from a small amount of sample material at the surface. Thus, it becomes important to know the absolute cross sections of different molecules adsorbed on surfaces, so that one may predict in advance if SRS is applicable for a given species of molecules.

In this paper we report on the measurement of the absolute Raman-scattering cross section of the symmetric NO_2 stretching vibration of an amorphous nitrobenzene layer at a frequency 1346 cm^{-1} . The sample was formed

by adsorption of nitrobenzene molecules on a clean and well-defined Ni(111) surface prepared in an ultrahigh vacuum (UHV). The range of thickness explored was from several monolayers to several hundred Å. This sample system was chosen, both because the nitrobenzene molecule has a very large Raman cross section and because we have sufficient information on the structure of this system.

To determine the absolute cross section, one must first calibrate the detection efficiency of the spectrometer system and measure the absolute intensity of the scattered light. One must also determine the molecular density and orientation on the substrate surface. The measured intensities depend on the Raman cross section and, in addition, on the incident and scattered angles, light polarizations, and the dielectric function of the substrate. Thus, to obtain the Raman cross section that is intrinsic to the sample system, it is necessary to sort out the optical effects of the environment. We will use a theory^{5,6} based on the electromagnetic Green's function to isolate the effect of the substrate on the propagation of incident and scattered light. This method of theoretical analysis is outlined in the next section.

When a molecule is adsorbed on a substrate, it binds with the surface atoms through electron interactions. As a result, the electronic state of the molecule will change, and consequently, the molecular Raman cross section will also change upon adsorption. This adsorbate-substrate interaction effect is expected to be appreciable only for the first few layers of the substrate. When the amount of adsorbate increases, a condensed phase forms with different possible local structures. The Raman cross section then starts to depend on the structure of the condensed phase as well as on the individual molecular cross section. Thus, the Raman cross section contains infor-

mation on both adsorbate-substrate and intermolecular interactions.

In our previous work^{1,2} we found that the nitrobenzene layer forms two different structures on Ni(111) depending on the substrate temperature. An amorphous structure occurs when the substrate temperature is held below 141 K. This phase irreversibly transforms into a crystalline phase above 145 K. In this work, we kept the temperature below 127 K to ensure that we had the amorphous phase.

This paper is organized in the following manner. Section II is an outline of the theory used to extract the electromagnetic effect of the substrate. In Sec. III we describe the calibration method for the spectrometer system efficiency, and in Sec. IV we present the details of the absolute Raman-scattering cross-section measurements. In Sec. V we describe the absolute Raman-scattering cross-section measurements of gaseous and liquid nitrobenzene. Section VI is the discussion of the results, and Sec. VII is the conclusion.

II. THEORY

A. Raman-scattering intensity from an adsorbed molecule

We consider the Raman-scattering process by surface-adsorbed molecules in three steps: (1) generation of local macroscopic electric fields at the molecular site by the incident laser light, (2) creation of an oscillating dipole through the Raman tensor, and (3) emission and propagation of the scattered light from the oscillating dipole. For simplicity, we initially consider Raman scattering from an isolated molecule on a substrate.

In the first step we need to know the local macroscopic electric field at the scattering molecule generated by the incident laser beam. We consider an arbitrary planar stack of dielectric layers as shown in Fig. 1. The scatter-

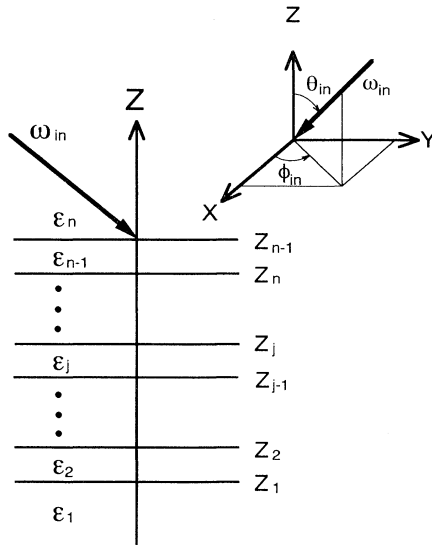


FIG. 1. Planar stack of dielectric layers and the laboratory coordinate system.

ing molecule may be embedded anywhere in this stack. When the exciting light of frequency ω_{in} is incident on the top medium [dielectric constant: $\epsilon_n(\omega)$] from the (θ_{in}, ϕ_{in}) direction with the wave vector

$$\mathbf{k}_n = - \left[\frac{\sqrt{\epsilon_n(\omega_{in})} \omega_{in}}{c} \right] \times (\sin\theta_{in}\cos\phi_{in}, \sin\theta_{in}\sin\phi_{in}, \cos\theta_{in}), \quad (1)$$

where c is the speed of light in a vacuum, the local macroscopic electric field $\mathbf{E}^{loc}(Z, \omega_{in})$ generated at the scattering molecule can be written as

$$\mathbf{E}^{loc}(Z, \omega_{in}) = \underline{A}(\theta_{in}, \phi_{in}, Z, \omega_{in}) \mathbf{E}^{in}(\omega_{in}). \quad (2)$$

$\mathbf{E}^{loc}(Z, \omega_{in}) = (E_X^{loc}, E_Y^{loc}, E_Z^{loc})$ is defined with respect to the laboratory frame, whose axes will be noted by the upper case letters $X, Y,$ and Z . $\underline{A}(\theta_{in}, \phi_{in}, Z, \omega_{in})$ is a 3×2 matrix based on the electromagnetic Green's function of the layered geometry. The explicit form of this matrix was given by Reed *et al.*⁵ $\mathbf{E}^{in}(\omega_{in})$ is the electric-field vector of the incident laser light written in terms of the s - and p -polarized components (E_S^{in}, E_P^{in}) with respect to the plane of incidence. These components are defined by

$$\begin{aligned} E_S^{in} &= \mathbf{E}^{in} \cdot \hat{\mathbf{S}} \text{ with } \hat{\mathbf{S}} = \frac{\mathbf{k} \times \hat{\mathbf{Z}}}{|\mathbf{k} \times \hat{\mathbf{Z}}|}, \\ E_P^{in} &= \mathbf{E}^{in} \cdot \hat{\mathbf{P}} \text{ with } \hat{\mathbf{P}} = \frac{\hat{\mathbf{S}} \times \mathbf{k}}{|\hat{\mathbf{S}} \times \mathbf{k}|}, \\ \mathbf{E}^{in} \cdot \mathbf{k} &= 0, \end{aligned} \quad (3)$$

where the quantities with carets are unit vectors.

The oscillating Raman dipole \mathbf{P} is related to the local macroscopic electric field at the scatterer through the Raman tensor of the scattering molecule α^L :

$$\mathbf{P}(Z, \omega_s) = \alpha^L \mathbf{E}^{loc}(Z, \omega_{in}), \quad (4)$$

where α^L is defined with respect to the laboratory frame. In this definition, the Raman tensor α^L contains the effects of the local microscopic field and the molecule-substrate and molecule-molecule interactions. Here, we note that the local electric field on the right-hand side of Eq. (4) is a macroscopic field that is an average of the microscopic field over a distance scale on the order of the wavelength.

The relation between the Raman tensors with respect to the laboratory frame and the internal coordinate of the molecule is given by

$$\alpha^L = \underline{C}^T(\Theta, \Phi, X) \alpha^m \underline{C}(\Theta, \Phi, X), \quad (5)$$

where α^m is the Raman tensor defined with respect to the molecular axes which will be denoted by the lower case letters $x, y,$ and z . $\underline{C}(\Theta, \Phi, X)$ is the direction cosine matrix that specifies the orientation of the molecular axes with respect to the laboratory frame, and $\underline{C}^T(\Theta, \Phi, X)$ is the transpose of $\underline{C}(\Theta, \Phi, X)$. $\underline{C}(\Theta, \Phi, X)$ is expressed by the Eulerian angles (Θ, Φ, X) .⁷

If the scattered electric field radiated by the oscillating Raman dipole is measured along the (θ_s, ϕ_s) direction far from the surface, it is given by

$$\mathbf{E}^{\text{out}}(\mathbf{r}, \omega_s) = \mathbf{E}^{\text{out}}(\theta_s, \phi_s, \mathbf{Z}, \omega_s) \frac{e^{i\mathbf{k}_n \cdot \mathbf{r}}}{r}. \quad (6)$$

The quantity $\mathbf{E}^{\text{out}}(\mathbf{r}, \omega_s)$ on the left-hand side is the electric-field vector [$E_S^{\text{out}}(\mathbf{r}, \omega_s)$, $E_P^{\text{out}}(\mathbf{r}, \omega_s)$] at position \mathbf{r} written in terms of the s - and p -polarized components. The quantity $\mathbf{E}^{\text{out}}(\theta_s, \phi_s, \mathbf{Z}, \omega_s)$ on the right-hand side is the amplitude vector of the scattered light. It is given by

$$\mathbf{E}^{\text{out}}(\theta_s, \phi_s, \mathbf{Z}, \omega_s) = \left[\frac{\omega_s}{c} \right]^2 \underline{\mathbf{A}}^T(\theta_s, \phi_s, \mathbf{Z}, \omega_s) \mathbf{P}(\mathbf{Z}, \omega_s), \quad (7)$$

where the matrix $\underline{\mathbf{A}}^T(\theta_s, \phi_s, \mathbf{Z}, \omega_s)$ is the transpose of $\underline{\mathbf{A}}(\theta_s, \phi_s, \mathbf{Z}, \omega_s)$ calculated for the scattered angle and frequency. The fact that the outgoing amplitude \mathbf{E}^{out} depends on the transpose of the same matrix $\underline{\mathbf{A}}$, which determines the incident local field \mathbf{E}^{loc} , follows directly from the Lorentz reciprocity theorem.⁵ From Eqs. (2), (4), and (7), the electric-field amplitude vector of the Raman-scattered light can be written as

$$\mathbf{E}^{\text{out}}(\theta_s, \phi_s, \mathbf{Z}, \omega_s) = \left[\frac{\omega_s}{c} \right]^2 \underline{\mathbf{A}}^T(\theta_s, \phi_s, \mathbf{Z}, \omega_s) \alpha^L \times \underline{\mathbf{A}}(\theta_{\text{in}}, \phi_{\text{in}}, \mathbf{Z}, \omega_{\text{in}}) \mathbf{E}^{\text{in}}(\omega_{\text{in}}). \quad (8)$$

When the Raman intensity is measured in the top medium, the intensity I^{out} per unit of solid angle is given by

$$\begin{aligned} I^{\text{out}} &= \left[\frac{c}{8\pi} \right] \left[\frac{\epsilon_n(\omega_s)}{\mu} \right]^{1/2} |\mathbf{e}^{\text{out}} \cdot \mathbf{E}^{\text{out}}(\omega_s)|^2 \\ &= \left[\frac{\omega_s}{c} \right]^4 \left[\frac{\epsilon_n(\omega_s)}{\epsilon_n(\omega_{\text{in}})} \right]^{1/2} \frac{I^{\text{in}}}{A_{\text{beam}}} \\ &\quad \times |\mathbf{e}^{\text{out}} \underline{\mathbf{A}}^T(\theta_s, \phi_s, \mathbf{Z}, \omega_s) \alpha^L \underline{\mathbf{A}}(\theta_{\text{in}}, \phi_{\text{in}}, \mathbf{Z}, \omega_{\text{in}}) \mathbf{e}^{\text{in}}|^2, \end{aligned} \quad (9)$$

where ϵ_n and μ are the dielectric constant and magnetic permeability of the top medium, and \mathbf{e}^{in} and \mathbf{e}^{out} are the incident and scattered polarization vectors, respectively. If the variation in the dielectric constant of the top layer over the frequency range of the Raman shift is ignored, the factor $\sqrt{\epsilon_n(\omega_s)/\epsilon_n(\omega_{\text{in}})}$ is unity.

In this formulation, the electromagnetic effect of the experimental geometry (i.e., the presence of a substrate in the present case) is contained in the matrices $\underline{\mathbf{A}}(\theta_{\text{in}}, \phi_{\text{in}}, \mathbf{Z}, \omega_{\text{in}})$ and $\underline{\mathbf{A}}^T(\theta_s, \phi_s, \mathbf{Z}, \omega_s)$. The properties of the substrate enter them through the dielectric constants of the different layers. When there is surface roughness we can use the matrices calculated by Sano, Mizutani, and Ushioda⁸ that include the effect of surface roughness in first-order perturbation.^{9,10} We can remove this purely optical factor from the measured intensities when we deduce the absolute Raman cross section.

B. Raman-scattering intensity from an adsorbed layer

Next, we consider the Raman-scattering intensity from an adsorbed layer on a substrate. Assuming that the scattering events are incoherent, the intensity can be expressed by the sum of contributions from each molecule,

$$\begin{aligned} I^{\text{out}} &= \left[\frac{\omega_s}{c} \right]^4 \left[\frac{\epsilon_n(\omega_s)}{\epsilon_n(\omega_{\text{in}})} \right]^{1/2} \frac{\rho_v I^{\text{in}}}{A_{\text{beam}}} \\ &\quad \times \int_v |\mathbf{e}^{\text{out}} \underline{\mathbf{A}}^T \alpha^L \underline{\mathbf{A}} \mathbf{e}^{\text{in}}|^2 dv, \end{aligned} \quad (10)$$

where v is the adsorbed layer volume that contributes to Raman scattering and ρ_v is the molecular number density.

To exhibit the relationship between the molecular orientation and the Raman tensor elements, we write the matrix product occurring in Eq. (10) in the form of a sum. Then, Eq. (10) becomes

$$I^{\text{out}} = \left[\frac{\omega_s}{c} \right]^4 \left[\frac{\epsilon_n(\omega_s)}{\epsilon_n(\omega_{\text{in}})} \right]^{1/2} \frac{\rho_v I^{\text{in}}}{A_{\text{beam}}} \sum_{I, J, K, L, I', J', K', L'} e_I^{\text{out}} e_L^{\text{in}} e_{I'}^{\text{out}} e_{L'}^{\text{in}} \int_{\mathbf{Z}} A_{IJ}^T A_{KL} A_{I'J'}^{T*} A_{K'L'}^* \left\{ \int_s \alpha_{JK}^L \alpha_{J'K'}^L dX dY \right\} dZ. \quad (11)$$

Anticipating that the layer is uniform in the XY plane, we have separated the integration over \mathbf{Z} . Next, we introduce the molecular orientation distribution function $f(\Theta, \Phi, X, \mathbf{Z})$ for the adsorbed layer. This function specifies the probability of finding a molecule oriented along the direction (Θ, Φ, X) at a height \mathbf{Z} from the substrate surface. We assume that it does not depend on the X and Y coordinates. This assumption is reasonable for adsorbed layers on smooth surfaces, because the strength of the interaction between the adsorbed molecule and the substrate depends only on the relative distance. $f(\Theta, \Phi, X, \mathbf{Z})$ is normalized to satisfy

$$\int_0^\pi \int_0^{2\pi} \int_0^{2\pi} f(\Theta, \Phi, X, \mathbf{Z}) \sin\Theta d\Theta d\Phi dX = 1. \quad (12)$$

Using this function, one can perform the integration in the XY plane and obtain

$$\begin{aligned} \int_s \alpha_{JK}^L \alpha_{J'K'}^L dX dY &= S \int_0^\pi \int_0^{2\pi} \int_0^{2\pi} \alpha_{JK}^L(\Theta, \Phi, X) \alpha_{J'K'}^L(\Theta, \Phi, X) f(\Theta, \Phi, X, \mathbf{Z}) \sin\Theta d\Theta d\Phi dX, \\ &= S \langle \alpha_{JK}^L \alpha_{J'K'}^L \rangle \end{aligned} \quad (13)$$

where $S = A_{\text{beam}}/\cos\theta_{\text{in}}$ and $\langle \alpha_{JK}^L \alpha_{J'K'}^L \rangle$ is a rotationally averaged binary product of the Raman tensor elements (referenced to the laboratory frame). As we will see later, it can be expressed in terms of the Raman tensor elements with respect to the internal molecular coordinates [see Eqs. (19) and (20)].

Using Eq. (13), we can rewrite Eq. (11) as

$$I^{\text{out}} = \left[\frac{\omega_s}{c} \right]^4 \left[\frac{\epsilon_n(\omega_s)}{\epsilon_n(\omega_{\text{in}})} \right]^{1/2} \frac{\rho_v I^{\text{in}}}{\cos\theta_{\text{in}}} \times \sum_{\substack{I,J,K,L \\ I',J',K',L'}} e_I^{\text{out}} e_L^{\text{in}} e_{I'}^{\text{out}} e_{L'}^{\text{in}} \times \int_{\mathbf{Z}} A_{IJ}^T A_{KL} A_{I'J'}^{T*} A_{K'L'}^* \langle \alpha_{JK}^L \alpha_{J'K'}^L \rangle d\mathbf{Z}. \quad (14)$$

If $f(\Theta, \Phi, X, Z)$ is independent of Z , then $\langle \alpha_{JK}^L \alpha_{J'K'}^L \rangle$ is also independent of Z , and Eq. (14) becomes

$$I^{\text{out}} = \left[\frac{\omega_s}{c} \right]^4 \left[\frac{\epsilon_n(\omega_s)}{\epsilon_n(\omega_{\text{in}})} \right]^{1/2} \frac{\rho_v I^{\text{in}}}{\cos\theta_{\text{in}}} \times \sum_{\substack{I,J,K,L \\ I',J',K',L'}} e_I^{\text{out}} e_L^{\text{in}} e_{I'}^{\text{out}} e_{L'}^{\text{in}} \langle \alpha_{JK}^L \alpha_{J'K'}^L \rangle \times \int_{\mathbf{Z}} A_{IJ}^T A_{KL} A_{I'J'}^{T*} A_{K'L'}^* d\mathbf{Z}. \quad (15)$$

This is the form of I^{out} that we will use in our analysis in the following sections.

C. Raman-scattering cross section of gases and liquids

To understand the details involved in defining the Raman cross section of adsorbed layers and molecules, it is useful first to consider how it is defined for gases and liquids, and to understand the relation between measured intensities and molecular Raman tensor elements. This relation results from rotational averaging.

Assuming that the sample size is sufficiently large, we use the $\underline{A}(\theta_{\text{in}}, \phi_{\text{in}})$ and $\underline{A}^T(\theta_s, \phi_s)$ matrices that describe the propagation of light in free space. Then, these matrices do not depend on the scatterer position and are given by

$$\underline{A}(\theta_{\text{in}}, \phi_{\text{in}}) = \begin{bmatrix} -\sin\theta_{\text{in}} & -\cos\theta_{\text{in}}\cos\phi_{\text{in}} \\ \cos\theta_{\text{in}} & -\cos\theta_{\text{in}}\sin\phi_{\text{in}} \\ 0 & \sin\theta_{\text{in}} \end{bmatrix} \quad (16)$$

and

$$\underline{A}^T(\theta_s, \phi_s) = \begin{bmatrix} -\sin\theta_s & \cos\theta_s & 0 \\ -\cos\theta_s\cos\phi_s & -\cos\theta_s\sin\phi_s & \sin\theta_s \end{bmatrix}. \quad (17)$$

Since gaseous and liquid states are isotropic, we can fix the direction and polarization of the incident light without loss of generality. We consider the geometry in which the incident direction is along the Z axis, $(\theta_{\text{in}}, \phi_{\text{in}}) = (0, 0)$, and the polarization is $\mathbf{e}^{\text{in}} = (0, 1, 0)$. In

this case, Eq. (15) becomes

$$I^{\text{out}} = \left[\frac{\omega_s}{c} \right]^4 \left[\frac{\epsilon(\omega_s)}{\epsilon(\omega_{\text{in}})} \right]^{1/2} \rho_v \Delta Z I^{\text{in}} \times \sum_{\substack{I,J \\ I',J'}} e_I^{\text{out}} e_{I'}^{\text{out}} \langle \alpha_{JY}^L \alpha_{J'Y}^L \rangle A_{IJ}^T(\theta_s, \phi_s) A_{I'J'}^{T*}(\theta_s, \phi_s), \quad (18)$$

where ΔZ is the length of the sample seen by the spectrometer, and $\epsilon(\omega)$ is the dielectric constant of the gas or liquid. The Raman-scattering intensity of gases and liquids in any experimental configuration can be calculated using Eqs. (17) and (18). The resulting expression for the Raman-scattering intensity depends on $\langle \alpha_{JY}^L \alpha_{J'Y}^L \rangle$, $\underline{A}^T(\theta_s, \phi_s)$, $\sqrt{\epsilon(\omega_s)/\epsilon(\omega_{\text{in}})}$, ρ_v , and ΔZ .

In gaseous and liquid states the molecules have random orientations. In this case, the rotational average $\langle \alpha_{JK}^L \alpha_{J'K'}^L \rangle$ can be expressed in terms of the Raman tensor elements with respect to internal molecular coordinates¹¹

$$\begin{aligned} \langle \alpha_{XX}^L \alpha_{YY}^L \rangle &= \langle \alpha_{YY}^L \alpha_{ZZ}^L \rangle = \langle \alpha_{ZZ}^L \alpha_{XX}^L \rangle = \frac{45a^2 + 4\gamma^2}{45}, \\ \langle \alpha_{XY}^L \alpha_{YZ}^L \rangle &= \langle \alpha_{YZ}^L \alpha_{ZX}^L \rangle = \langle \alpha_{ZX}^L \alpha_{XY}^L \rangle = \frac{\gamma^2}{15}, \\ \langle \alpha_{XX}^L \alpha_{YY}^L \rangle &= \langle \alpha_{YY}^L \alpha_{ZZ}^L \rangle = \langle \alpha_{ZZ}^L \alpha_{XX}^L \rangle = \frac{45a^2 - 2\gamma^2}{45}, \end{aligned} \quad (19)$$

otherwise 0,

where a^2 and γ^2 are defined by

$$\begin{aligned} a^2 &= \frac{1}{9}(\alpha_{xx}^m + \alpha_{yy}^m + \alpha_{zz}^m)^2, \\ \gamma^2 &= \frac{1}{2}\{(\alpha_{xx}^m - \alpha_{yy}^m)^2 + (\alpha_{yy}^m - \alpha_{zz}^m)^2 \\ &\quad + (\alpha_{zz}^m - \alpha_{xx}^m)^2 + 6(\alpha_{xy}^{m2} + \alpha_{yz}^{m2} + \alpha_{zx}^{m2})\}. \end{aligned} \quad (20)$$

In the above expressions, the α_{ij}^m 's are the molecular Raman tensor elements defined with respect to the internal coordinate of the molecule (x, y, z). If we know a^2 and γ^2 , we can calculate the Raman-scattering intensity of the gas or liquid for an arbitrary scattering geometry.

The Raman-scattering cross section for gases and liquids is defined by the ratio of the scattered light intensity to the incident light intensity, when the incident light propagates along the Z axis with polarization along Y , and the scattered light is observed along the X axis with the same polarization. In this scattering configuration, the Raman-scattering intensity is given by

$$I^{\text{out}} = \left[\frac{\omega_s}{c} \right]^4 \left[\frac{\epsilon(\omega_s)}{\epsilon(\omega_{\text{in}})} \right]^{1/2} \rho_v \Delta Z \langle \alpha_{YY}^L \rangle I^{\text{in}}. \quad (21)$$

There are two different definitions of the Raman-scattering cross section. One is the power cross section σ_p , which is defined by $\sigma_p = (\text{power of scattered light per molecule})/(\text{power of incident light per unit area})$. The other is the quantum cross section σ_q , where $\sigma_q = (\text{number of scattered photons per molecule})/(\text{number of incident photons per unit area})$. In this paper,

we use the latter definition, since it is more convenient when the intensity is measured by photon counting. Thus, we use the differential Raman-scattering cross section defined by

$$\frac{d\sigma}{d\Omega} = \frac{d\sigma_q}{d\Omega} = \left[\frac{\omega_s^3 \omega_{in}}{c^4} \right] \langle \alpha_{YY}^L{}^2 \rangle. \quad (22)$$

This definition is slightly different from that used by Skinner and Nilsen,¹² and Kato and Takuma,¹³ theirs is equal to our cross section multiplied by $\sqrt{\epsilon(\omega_s)/\epsilon(\omega_{in})}$. Since $\sqrt{\epsilon(\omega_s)/\epsilon(\omega_{in})}$ is almost equal to unity when the energies of the incident and scattered photons are far from the electronic transition energies of the molecule, these two cross sections are nearly equal except for the case of resonant Raman scattering.

The depolarization ratio ρ is defined by

$$\rho = \frac{\langle \alpha_{ZY}^L{}^2 \rangle}{\langle \alpha_{YY}^L{}^2 \rangle}. \quad (23)$$

Since a^2 and γ^2 can be calculated from $d\sigma/d\Omega$ and ρ , these two parameters are sufficient to describe the Raman-scattering intensity of gases and liquids completely. We note in passing that the Raman tensor elements α_{ij}^m with respect to the molecular axes can never be determined from experiments for gases and liquids. From the symmetry of the molecule, one can determine theoretically which elements are nonzero, but the numerical ratios among them cannot be experimentally determined.

From $d\sigma/d\Omega$ and ρ we can calculate the total Raman cross section σ , which is expressed by

$$\sigma = \frac{8\pi}{3} (1+2\rho) \frac{d\sigma}{d\Omega}. \quad (24)$$

Although the differential Raman cross section is more convenient for experiments than the total cross section, we use the total Raman cross section when we compare the cross sections of molecules in different states.

D. Raman-scattering cross section of an adsorbed layer

Finally, we wish to define the Raman cross section for an adsorbed layer. A simple and straightforward definition is possible, if the molecular orientation in the adsorbed layer is random throughout the thickness of the layer. This is true if the layer is amorphous and the effect of adsorbate-substrate interactions at the interface can be neglected. Then, Eq. (15) represents the Raman intensity for the layer. The rotationally averaged binary products of Raman tensor elements are the same as for the gaseous or liquid phases. Thus, the differential Raman cross section, the depolarization ratio, and the total Raman cross section can be defined by Eqs. (22), (23), and (24), respectively. In this especially simple case the total Raman cross section of the adsorbed layer can be compared directly with that of the gas or the liquid. In the present work we need to deal only with this simple case.

If the molecular orientation distribution $f(\Theta, \Phi, X, Z)$ depends on the distance Z from the surface, one can consider every monolayer to be a separate layer, and proceed to define the cross section for each monolayer. This is

possible in principle, but it would be extremely difficult experimentally to untangle the cross sections in this situation.

Even when the molecular orientation distribution is independent of the distance from the substrate surface, in general it is not random. Then, we need to know all of the rotationally averaged binary products $\langle \alpha_{JK}^L \alpha_{J'K'}^L \rangle$ in order to predict the Raman intensity for an arbitrary scattering configuration. We must define differential cross sections for the adsorbed layer by

$$\frac{d\sigma_{JKJ'K'}}{d\Omega} = \left[\frac{\omega_s^3 \omega_{in}}{c^4} \right] \langle \alpha_{JK}^L \alpha_{J'K'}^L \rangle \quad (25)$$

for each polarization combination. This is the situation encountered in anisotropic crystals. The necessary number of independent Raman cross sections depends on the structure of the adsorbed layer. For example, the number is only two for an amorphous layer, as we have seen above, and five for a uniaxial layer.

The cross section we have defined in this section represents a macroscopic averaged property of the adsorbed layer rather than the cross section of individual molecules. When the density of adsorbates is large enough to cause strong interactions among them and consequent formation of a crystalline or amorphous structure, the cross section of the layer is determined by its structure as well as individual molecular cross sections. Hence, we are dealing with the cross section of the condensed phase, even though we may still calculate formally the cross section per formula unit. There appears to be no theory in the literature that relates molecular Raman cross sections to those of the condensed phases formed by the same molecules.

If the density of the adsorbates is small and the interaction among them is weak, one can obtain a meaningful cross section for individual adsorbed molecules. However, in general, the cross sections of adsorbed layers and adsorbed molecules cannot be directly compared with those of gases and liquids, because the molecular orientation distribution function is different for the different phases. Only when the molecular orientations in the adsorbed layer are known or are completely random can one compare the cross sections of the adsorbed layer with that of gaseous or liquid phases.

III. MEASUREMENT OF THE RAMAN SPECTROMETER SYSTEM EFFICIENCY

The Raman spectrometer utilized in the experiments is a computer-controlled Jobin-Yvon U-1000 double monochromator equipped with a cooled Hamamatsu R649 photomultiplier tube. The dark count rate of this tube is less than 1 cps at -30°C . To obtain the absolute Raman-scattering intensity, we have determined the absolute detection efficiency of our spectrometer system. In this section we describe the method of efficiency calibration and evaluation of the effective solid angle of the input optics.

A. Calibration of spectrometer efficiency

A halogen standard lamp (Ushio JDP100-500CS) was used as the light source in this set of measurements. The radiation intensity of this lamp is calibrated at 50 cm from the filament within an uncertainty of $\pm 3\%$. The first step was the calibration of the transmission coefficients of neutral density (ND) filters that were used to attenuate the light entering the spectrometer. We used four ND filters, three with $\frac{1}{8}$ nominal attenuation, and one with $\frac{1}{4}$ nominal attenuation. The transmission of the individual ND filters was measured by photon counting at a fixed wavelength of 5145 Å. The experimental uncertainty of the combined transmission of the four ND filters was $\pm 0.6\%$.

The standard lamp was placed exactly 50 cm from the spectrometer entrance slit, and the calibrated set of ND filters was inserted in front of the entrance slit. The number of incident photons into the spectrometer was calculated from the calibrated radiation intensity, the ND filter transmission coefficient, the entrance slit area, and the dispersion of the spectrometer. From the calculated incident photon number and the detected photon number, we obtained the absolute efficiency of our spectrometer system including the spectrometer and the photomultiplier tube. The efficiencies are 1.08% and 0.433% for *p* and *s* polarizations, respectively, at 5145 Å. The *s* and *p* polarizations are defined with respect to the reflection plane of the gratings. These values do not include the transmission efficiency of the input optics. The measurement uncertainty is $\pm 11\%$.

Next, we measured the efficiency of our spectrometer system as a function of wavelength. In this step, we cannot use ND filters because their transmission may have wavelength dependence. Thus, we inserted a very small pinhole between the bulb and the entrance slit of the spectrometer in order to attenuate the light. In this geometry we can only measure the relative efficiency as a function of the wavelength. From the absolute efficiency at 5145 Å and the relative efficiency as a function of wavelength, we determined the absolute efficiency of our spectrometer system for the entire spectral range of the system as shown in Fig. 2. The experimental uncertainty here is $\pm 15\%$.

To verify the absolute efficiency calibration, we measured the absolute differential Raman-scattering cross

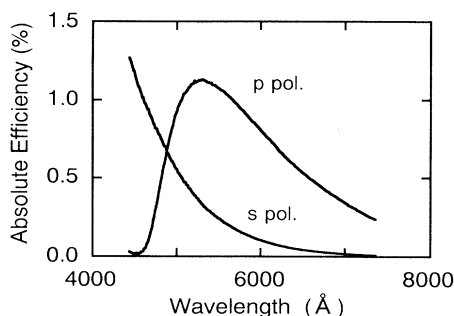


FIG. 2. Absolute efficiency of our Raman spectrometer system as a function of wavelength for *s* and *p* polarizations.

section of liquid benzene which has been previously measured.^{12,13} Our result is $3.10 \times 10^{-29} \text{ cm}^2/(\text{molecule sr line plane of polarization})$. (This unit refers to the integrated intensity over the entire line width.) This value agrees very well with the values in the literature. Thus, we are confident that both the standard lamp and the spectrometer are correctly calibrated.

B. Effective solid angle of collection

To obtain absolute cross sections one must measure absolute Raman-scattering intensities for a precisely known solid angle of collection. Our input optics were carefully designed to minimize the aberration loss, using two achromatic lenses under the infinite conjugate ratio condition. However, the aberration loss still occurs for light rays that pass near the rims of the lenses. Hence, the effective solid angle of collection is less than the value determined by geometrical factors. Thus, it was necessary to evaluate the effective solid angle for input optics.

For this purpose, we measured the Raman-scattering intensity of liquid nitrobenzene in the right-angle scattering geometry. First, we measured the intensity I_a by collecting only paraxial rays. In this measurement, we inserted a small aperture to allow only paraxial rays to pass through the input optics. The solid angle $\Delta\Omega_a$ was determined geometrically. Next, we measured the Raman intensity I_0 of the same sample without the aperture. Then the effective solid angle of collection $\Delta\Omega_{\text{eff}}$ is given by

$$\Delta\Omega_{\text{eff}} = \frac{I_0}{I_a} \Delta\Omega_a. \quad (26)$$

The measured value of $\Delta\Omega_{\text{eff}}$ was 0.0238 sr at 5223 Å where the 1346-cm^{-1} line of nitrobenzene appears on the Stokes side shifted from the incident laser line at 4880 Å. This value of $\Delta\Omega_{\text{eff}}$ was used when we calculated absolute Raman-scattering cross sections. The measurement uncertainty in $\Delta\Omega_{\text{eff}}$ is $\pm 3.7\%$.

IV. RAMAN MEASUREMENTS

A. Experimental setup

The experiments were performed using a stainless-steel ultrahigh-vacuum (UHV) chamber and a Raman spectrometer system that have been previously described.^{1,2} The UHV chamber is equipped with standard apparatus for surface cleaning and characterization, and a manipulator with liquid-nitrogen cooling and tungsten-wire heating capabilities. For calibration of the coverage of nitrobenzene a cylindrical mirror analyzer (CMA) Auger apparatus was used. The chamber was operated at a base pressure of 4×10^{-10} Torr.

The preparation of the Ni(111) substrate is described in our previous papers.^{1,2} Nitrobenzene was adsorbed onto the Ni(111) surface at the partial pressure of 1.0×10^{-7} Torr. This pressure reading is not corrected for ion gauge sensitivity. During the adsorption of nitrobenzene and the Raman measurements, the substrate temperature was kept below 127 K by liquid-nitrogen cooling to ensure the formation of an amorphous layer.

We used the 4880-Å line of an argon-ion laser as the exciting light source for the Raman measurements. The incident beam impinged through a spherical lens of focal length 250 mm onto the sample. When the polarization of the Raman-scattered light was analyzed, we inserted a depolarizer between the entrance slit of the spectrometer and the input lenses to eliminate the difference of the spectrometer efficiency for different polarizations. A polarization analyzer was inserted between the two input lenses. For absolute Raman intensity measurements we used neither an analyzer nor a depolarizer, and the resolution of the spectrometer was set at 24 cm^{-1} (slit width = 2.7 mm).

B. Coverage calibration

In our previous paper² we described in detail the coverage calibration of nitrobenzene adsorbed on a Ni(111) surface at substrate temperatures below 140 K. Using the CMA Auger apparatus we measured the Auger intensity of carbon at 272 eV (C_{272}) as a function of exposure up to a few monolayers. The result is plotted in Fig. 3. The break in this plot at 5.5 L (1×10^{-6} Torr sec; uncorrected for ion gauge sensitivity) is indicative of monolayer formation. Under the assumptions that this break is caused by a change of the sticking coefficient, that the sticking coefficient is constant after the first monolayer is formed, and further that the molecular number density of each successive monolayer is a constant equal to that of the first monolayer, we conclude that a monolayer is formed every 16.7 L after the first monolayer.

To determine the molecular number density of the adsorbed layer, we argue as follows. In our previous work² we found that only a monolayer of nitrobenzene is chemisorbed on Ni(111) at room temperature. Also, carbon monoxide (CO) is known to form a chemisorbed monolayer at room temperature with the $c(4 \times 2)$ structure¹⁴ and with a coverage of 0.5 relative to the Ni(111) surface atoms. Accordingly, the molecular number density of the first nitrobenzene monolayer can be calculated from the ratio of the Auger intensity of carbon in nitrobenzene to that of carbon in CO at saturated coverage at room temperature. We found the Auger intensity ratio, $I_{\text{nitrobenzene}}/I_{\text{CO}}$, to be 1.70. Since nitrobenzene has six

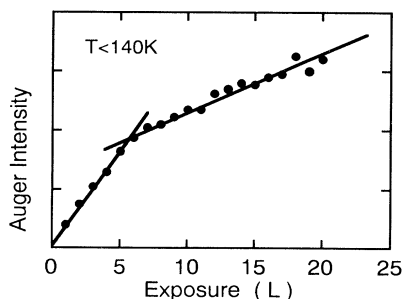


FIG. 3. Auger peak intensity for carbon 272 eV vs exposure of nitrobenzene to the Ni(111) surface at a substrate temperature below 140 K (Ref. 2). The backfilling pressure for exposure was 2×10^{-8} Torr.

carbon atoms while CO has one carbon atom, the molecular number density of the first nitrobenzene layer on Ni(111) is 2.63×10^{14} molecules/cm² layer. The measurement uncertainty is $\pm 14\%$.

C. Layer thickness from reflectivity measurements

For the calculation of the \underline{A} and \underline{A}^T matrices, we need both the relation between exposure and layer thickness, and the dielectric constant of the amorphous nitrobenzene layer. We obtained these data from the measurement of reflectivity as a function of exposure. The measurements were made at two different wavelengths, 4880 and 5145 Å, with the incident angle 50° from the surface normal. Knowing the dielectric constant of Ni at 4880 and 5145 Å to be $-7.0 + i11.6$ and $-7.9 + i12.4$, respectively,¹⁵ one can calculate the reflectivity of the vacuum/nitrobenzene layer/Ni(111) structure.¹⁶ The dielectric constant of the amorphous nitrobenzene layer was assumed to be real and constant around 5000 Å. We determined both the relationship between exposure and layer thickness, and the dielectric constant, by fitting the reflectivity data to the calculated result by the method of least-squares fitting. The fitting results are shown in Fig. 4 for the two wavelengths. We obtained the relation that 2.8-L exposure is equivalent to a 1-Å layer thickness. The dielectric constant of the amorphous nitrobenzene

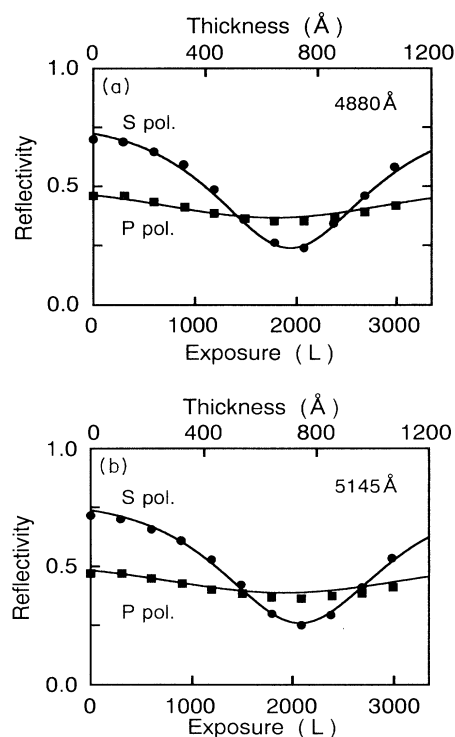


FIG. 4. Reflectivity of the amorphous nitrobenzene layer on Ni(111) as a function of exposure at a substrate temperature below 130 K, (a) at 4880 Å and (b) at 5145 Å. The incident angle was 50° . The top horizontal scale denotes the layer thickness determined by a fitting procedure. The solid curves correspond to the calculated results.

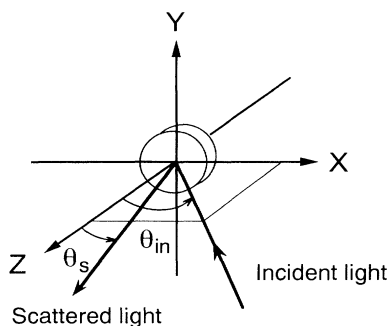


FIG. 5. Scattering geometry for the Raman intensity measurements. XYZ coordinates are for the laboratory frame. θ_{in} and θ_s are the incident and scattered angles, respectively.

layer was found to be 2.5. Assuming that the molecular density of the upper monolayers is the same as that of the first monolayer, we can obtain the molecular number density of the amorphous nitrobenzene layer, which is 4.4×10^{21} molecules/cm³.

D. Exposure dependence of Raman intensity

We measured the absolute Raman intensity of the NO₂ symmetric stretching mode (1346 cm^{-1}) of the amorphous nitrobenzene layer as a function of exposure. The substrate temperature was kept below 127 K to keep the layer in an amorphous state. The scattering geometry is shown in Fig. 5. The plane of incidence coincides with the XZ plane. The incident beam at 4880 \AA was directed onto the sample surface at 45° from the surface normal and the scattered light was collected along the surface normal. The incident power at the viewing port of the UHV chamber was 150 mW. We define the polarization

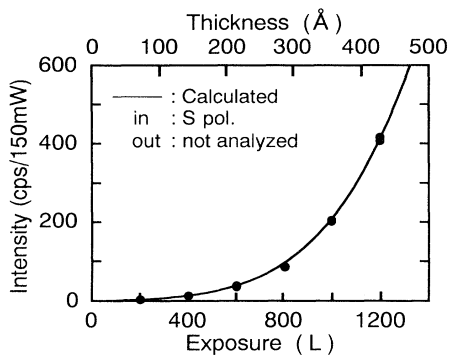


FIG. 6. Measured Raman-scattering intensity of the NO₂ symmetric stretching mode from the amorphous nitrobenzene layer on Ni(111) as a function of exposure. The incident power was 150 mW at the viewing port of the UHV chamber and the wavelength was 4880 \AA . The incident and scattered angles were 45° and 0° , respectively. The incident light was s polarized and the scattered light was not analyzed. The spectrometer resolution was set at 24 cm^{-1} , and the effective solid angle of collection was 0.0238 sr . The Raman cross section was obtained by fitting the solid calculated curve to the data points. The top horizontal scale denotes layer thickness.

of the scattered light with respect to the plane of incidence. The electric field of the s -polarized scattered light in this geometry has only a Y component. The absolute Raman intensity was measured for various exposures at intervals of 200 L in the range of 200–1200 L. The solid circles in Fig. 6 show the measured Raman intensity as a function of exposure when the exciting light is s polarized and the scattered light is not analyzed.

We measured Raman intensity ratios as a function of exposure for all combinations of the incident and scattered polarizations. The results for the polarized intensity ratios are shown in Fig. 7. The first and second subscripts on I in Fig. 7 refer to the incident and scattered polarizations, respectively. In Figs. 6 and 7 the solid curves were calculated from the absolute Raman cross section and the depolarization ratio. The procedure for obtaining these two quantities will be described in the next section. Figure 8 illustrates the Raman spectrum of the NO₂ symmetric stretching mode of an amorphous nitrobenzene layer (1200 L) adsorbed on Ni(111) below 127 K. The observation of a single asymmetric peak indicates that the adsorbed layer is in an amorphous state.¹

E. Absolute Raman cross section

In this section we describe the process of determining the absolute Raman cross section and depolarization ratio from the results shown in Figs. 6 and 7. The depolarization ratio can be directly obtained from the intensity ratio I_{sp}/I_{ss} in Fig. 7. To show this we derive the relation between the intensity ratio I_{sp}/I_{ss} and the depolarization ratio. The Green's-function matrix $\underline{A}^T(0,0,Z,\omega_s)$ for the emitted beam for $\theta_s = \phi_s = 0^\circ$ is given by

$$\begin{aligned} \underline{A}^T(0,0,Z,\omega_s) &= \begin{bmatrix} 0 & A_{SY}(Z,\omega_s) & 0 \\ A_{PX}(Z,\omega_s) & 0 & 0 \end{bmatrix}, \\ &= \begin{bmatrix} 0 & A_{PX}(Z,\omega_s) & 0 \\ A_{PX}(Z,\omega_s) & 0 & 0 \end{bmatrix}, \end{aligned} \quad (27)$$

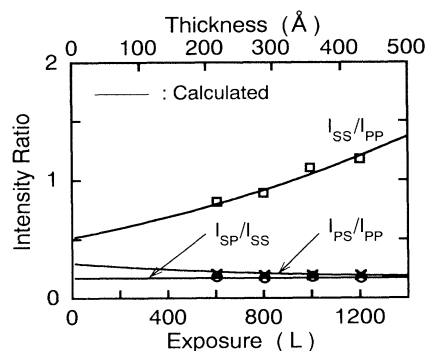


FIG. 7. Raman intensity ratios for the incident and scattered polarization combinations as a function of exposure. The subscripts on I correspond to the incident and scattered light polarizations in that order. The scattering geometry was the same as that of Fig. 6. The solid curves represent the calculated results from the Raman cross section and depolarization ratio. The top horizontal axis denotes layer thickness.

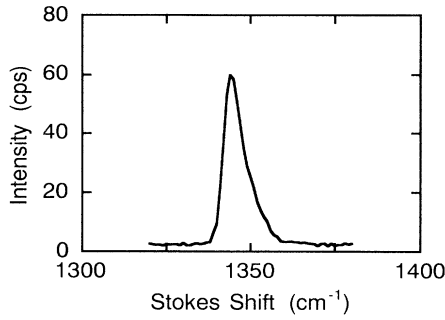


FIG. 8. Raman spectrum of the NO₂ symmetric stretching mode of the amorphous nitrobenzene layer (1200 L) on Ni(111) below 127 K. The spectrometer resolution was set at 2.7 cm⁻¹.

where $A_{SY}(Z, \omega_s)$ is equal to $A_{PX}(Z, \omega_s)$, because the emission is normal to the surface. The Green's-function matrix $\underline{A}(45^\circ, 0, Z, \omega_{in})$ for the incident side for $\theta_{in}=45^\circ$, $\phi_{in}=0^\circ$ is given by

$$\underline{A}(45^\circ, 0, Z, \omega_{in}) = \begin{pmatrix} 0 & A_{XP}(Z, \omega_{in}) \\ A_{YS}(Z, \omega_{in}) & 0 \\ 0 & A_{ZP}(Z, \omega_{in}) \end{pmatrix}. \quad (28)$$

Thus, when s -polarized exciting light impinges on the surface and the Raman-scattered light is observed along the surface normal, the intensity ratio of I_{SP}/I_{SS} is

$$\begin{aligned} \frac{I_{SP}}{I_{SS}} &= \frac{\int_0^d A_{PX}^2(Z, \omega_s) \langle \alpha_{XY}^2 \rangle A_{YS}^2(Z, \omega_{in}) dZ}{\int_0^d A_{SY}^2(Z, \omega_s) \langle \alpha_{YY}^2 \rangle A_{YS}^2(Z, \omega_{in}) dZ} \\ &= \frac{\langle \alpha_{XY}^2 \rangle}{\langle \alpha_{YY}^2 \rangle} = \rho, \end{aligned} \quad (29)$$

where we assumed that the rotationally averaged binary products of the Raman tensor elements, $\langle \alpha_{YY}^2 \rangle$ and $\langle \alpha_{XY}^2 \rangle$, do not depend on the Z coordinate in the amorphous layer. We see that the intensity ratio I_{SP}/I_{SS} is independent of the layer thickness and that it is a property of the amorphous layer. Experimentally, the intensity ratio I_{SP}/I_{SS} is constant over the exposure range from 600 to 1200 L as seen in Fig. 7. The depolarization ratio of amorphous nitrobenzene layer is equal to 0.17.

Using this depolarization ratio in conjunction with Eqs. (19) and (23), we can determine the relative ratios of all of the rotationally averaged binary products of Raman tensor elements. Since we have obtained all the necessary parameter values such as the dielectric constant and the proportionality constant between exposure and layer thickness, we can now calculate the matrix elements of \underline{A} and \underline{A}^T . The only number yet undetermined is the absolute cross section.

The absolute differential Raman cross section was determined by the following fitting procedure. The observed Raman intensity is obtained by multiplying Eq. (10) by the efficiency of the spectrometer η_{mono} , the effective solid angle of collection $\Delta\Omega_{eff}$, and the transmission coefficient of the viewing port of the UHV chamber

β ,

$$I^{ob} = \eta_{mono} \Delta\Omega_{eff} \beta \frac{\omega_s^3 \omega_{in}}{c^4} \left[\frac{\epsilon_n(\omega_s)}{\epsilon_n(\omega_{in})} \right]^{1/2} \frac{\rho_v I^{in}}{A_{beam}} \times \int_v |\mathbf{e}^{out} \underline{A}^T \alpha^L \underline{A} \mathbf{e}^{in}|^2 dv, \quad (30)$$

where I^{ob} and I^{in} are the observed and incident intensities in units of photons/sec. Using the absolute differential cross section as the fitting parameter in Eq. (30), we fit the measured Raman intensity as a function of exposure. The best fit, which was determined by the method of least-squares fitting, is illustrated in Fig. 6 by the solid curve; the fit is excellent. From this procedure we obtained the absolute differential Raman-scattering cross section

$$\frac{d\sigma}{d\Omega} = 3.7 \times 10^{-28} \text{ cm}^2/\text{molecule sr line plane}$$

of polarization .

Then, the total Raman cross section as defined by Eq. (24) is

$$\sigma = 4.2 \times 10^{-27} \text{ cm}^2/\text{molecule line}.$$

The uncertainty in the cross section is estimated to be $\pm 34\%$. This uncertainty arises from the errors in determining the scattered photon number ($\pm 1.5\%$), the incident photon number ($\pm 2.0\%$), the surface molecular density ($\pm 14\%$), the effective solid angle of collection ($\pm 3.7\%$), the efficiency of the spectrometer ($\pm 11\%$), and the dielectric constant ($\pm 2.4\%$).

From the absolute differential Raman cross section and the depolarization ratio one can predict Raman intensities for any scattering configuration. As a check on our result we measured the absolute Raman intensity and po-

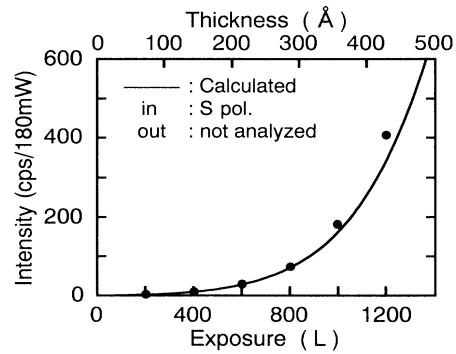


FIG. 9. Measured Raman-scattering intensity of the NO₂ symmetric stretching mode as a function of exposure. The incident power was 180 mW at the viewing port of the UHV chamber and the wavelength was 4880 Å. The incident and scattered angles were 60° and 30°, respectively. The incident light was s polarized and the scattered light was not analyzed. The spectrometer resolution was set at 24 cm⁻¹, and the effective solid angle of collection was 0.0238 sr. The solid curve was calculated from the Raman cross section and depolarization ratio determined from the data obtained at $\theta_{in}=45^\circ$, $\theta_s=0^\circ$. The top horizontal axis denotes layer thickness.

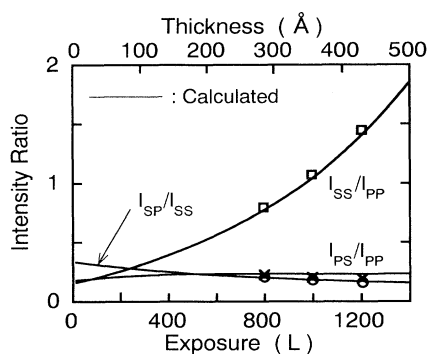


FIG. 10. Raman intensity ratios for the incident and scattered light polarization combinations as a function of exposure. The subscripts on I correspond to the incident and scattered polarizations in that order. The scattering geometry was the same as that of Fig. 9. The solid curves were calculated from the Raman cross section and depolarization ratio determined from the data obtained at $\theta_{in}=45^\circ$, $\theta_s=0^\circ$. The top horizontal axis denotes layer thickness.

larized intensity ratios for another scattering geometry; the incident and scattered angles were 60° and 30° , respectively. The results are shown in Figs. 9 and 10. The theoretical curves were calculated for this new scattering geometry from the absolute differential cross section and the depolarization ratio determined at $\theta_{in}=45^\circ$ and $\theta_s=0^\circ$. We emphasize that there is no adjustable parameter in the plots of Figs. 9 and 10. The calculated results reproduce the experimental data extremely well. Thus, we have clearly verified that our data are consistent and sufficiently accurate.

In Fig. 10 polarization data for the low coverage region are absent because we could not obtain those points due to low signal levels. However, we could obtain the unpolarized intensities even in the low coverage region as seen in Fig. 9.

V. RAMAN CROSS SECTIONS OF GASEOUS AND LIQUID NITROBENZENE AND BENZENE

To check the calibration of our spectrometer system and also to compare the Raman cross section of nitrobenzene in the three different phases, gas, liquid, and amorphous, we have measured the absolute Raman-scattering intensity of gaseous and liquid nitrobenzene and benzene in a right-angle scattering geometry. The scattering geometry in the laboratory frame is shown in Fig. 11. The incident laser beam at 4880 \AA was focused with a spherical lens of focal length 60 mm. It was polarized along the Z axis. The scattered light was collected along the X axis. When the scattered light is not analyzed, the observed Raman-scattering intensity I^{ob} integrated over the peak area in this scattering geometry is expressed by

$$I^{ob} = \eta_{para} \Delta\Omega \beta \Delta Z \left[1 + \frac{\eta_{per}}{\eta_{para}} \rho \right] \rho_v \frac{d\sigma}{d\Omega} I^{in}, \quad (31)$$

where $d\sigma/d\Omega$ is the absolute differential Raman-

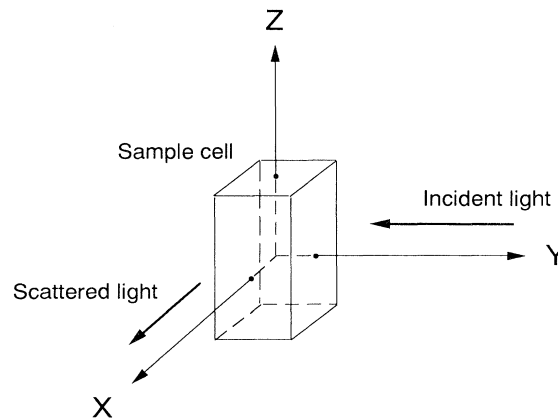


FIG. 11. The scattering geometry and the laboratory frame for the Raman measurements of gases and liquids.

scattering cross section per molecule per unit solid angle; ρ is the depolarization ratio; η_{para} and η_{per} are the detection efficiencies of the spectrometer system for the polarized and depolarized scattered light, respectively; β is the correction factor for reflections at the sample cell walls and absorption of the liquid sample; ρ_v is the molecular number density of the sample; and ΔZ is the image length of the spectrometer slit at the sample. $\Delta\Omega$ is the geometrical solid angle of collection. We inserted a small aperture between the sample cell and the input optics to prevent the aberration loss and a resultant uncertainty in the solid angle of collection. The solid angle was determined from the distance between the illuminated sample volume and the aperture, the aperture radius, and the refractive index of the sample. We assumed that the refractive index of the dilute gas is equal to unity.

From the absolute intensities of incident and scattered light and the depolarization ratio, the absolute Raman-scattering cross sections of nitrobenzene in the gaseous and liquid states were determined. The results for liquid nitrobenzene are

$$\left. \frac{d\sigma}{d\Omega} \right|_{liquid} = 8.51 \times 10^{-29} \text{ cm}^2/\text{molecule sr line plane}$$

of polarization

and

$$\rho = 0.175.$$

From these values and Eq. (24) the total Raman cross section σ_{liquid} is

$$\sigma_{liquid} = 9.62 \times 10^{-28} \text{ cm}^2/\text{molecule line}.$$

It was very difficult to measure the depolarization ratio of gaseous nitrobenzene accurately since the vapor pressure is very low at room temperature. Thus, we assume that the depolarization ratio of gaseous nitrobenzene is the same as that of the liquid in calculating the absolute Raman cross section. This assumption is reasonable, because the form of the Raman tensor is expected to remain the same. The differential and total Raman cross sections

of gaseous nitrobenzene are the following:

$$\left(\frac{d\sigma}{d\Omega} \right)_{\text{gas}} = 1.27 \times 10^{-29} \text{ cm}^2/\text{molecule sr line plane}$$

of polarization

and

$$\sigma_{\text{gas}} = 1.44 \times 10^{-28} \text{ cm}^2/\text{molecule line} ,$$

respectively.

We also measured the absolute Raman-scattering cross sections and depolarization ratios of benzene in the gaseous and liquid states. The values for gaseous benzene are the following:

$$\left(\frac{d\sigma}{d\Omega} \right)_{\text{gas}} = 9.66 \times 10^{-30} \text{ cm}^2/\text{molecule sr line plane}$$

of polarization ,

$$\sigma_{\text{gas}} = 8.25 \times 10^{-29} \text{ cm}^2/\text{molecule line} ,$$

and

$$\rho_{\text{gas}} = 0.010 .$$

The values for liquid benzene are the following:

$$\left(\frac{d\sigma}{d\Omega} \right)_{\text{liquid}} = 3.10 \times 10^{-29} \text{ cm}^2/\text{molecule sr line plane}$$

of polarization ,

$$\sigma_{\text{liquid}} = 2.70 \times 10^{-28} \text{ cm}^2/\text{molecule line} ,$$

and

$$\rho_{\text{liquid}} = 0.019 .$$

The differential Raman cross sections of liquid nitrobenzene and benzene were previously measured by Skinner and Nilsen¹² and Kato and Takuma.¹³ Our results agree with their results within experimental uncertainty. This result further verifies the consistency of our measurements.

VI. DISCUSSION

The most important objective of the present work was to define and actually measure the absolute Raman-scattering cross section for a surface-adsorbed layer. In contrast to the case of isotropic bulk media where this can be done in a straightforward manner, it was necessary to take careful account of the optical effects of the substrate and the layer geometry; only by doing this could we obtain the Raman cross section, which is a property solely of the adsorbate layer. We verified that the cross section we obtained is indeed a property solely of the amorphous nitrobenzene layer by predicting the Raman intensity for another arbitrary scattering geometry and finding that the prediction matched the measurement. We have demonstrated that all the parameters (i.e., layer thickness, dielectric constant, and molecular number density) necessary for determination of the

cross section can be obtained *in situ* for an ultrathin layer in UHV. We believe this is the first time that a complete measurement and analysis of the Raman cross section of a very thin adsorbed layer has been carried out.

Let us now consider the factors that determine the difference between the cross sections for the gaseous, liquid, and amorphous adsorbed states. The observed ratio between gas, liquid, and amorphous adsorbed phases (1:7:29) refers to cross sections per formula unit. Thus, the differences in molecular number density are automatically taken into account. The change in the cross section between phases can arise through two distinct mechanisms: intermolecular interactions and microscopic local electric fields, both of which depend on the molecular density.¹⁷⁻¹⁹ When the molecular density changes the strength of the interactions between the molecules changes. This change in intermolecular interactions affects the molecular polarizability and its derivatives, i.e., the Raman tensor elements. This is an intrinsic change of the molecular property caused by interactions with other molecules. At present we are not aware of theories to deal with this issue quantitatively.

The second mechanism arises from the fact that we are using light as the probe. The *microscopic* local field that is felt by individual molecules depends on the arrangement of other molecules around it. The local *macroscopic* field that was calculated in Eq. (2) is the average of the *microscopic* field over a volume comparable to the cube of the wavelength. Thus, we remarked earlier that the effect of the difference between the true *microscopic* field felt by a molecule and the *macroscopic* field is implicitly contained in the definition of the Raman tensor α^L . Part of the measured difference in the cross section per formula unit must arise from this source.

Eckhardt and Wagner²⁰ proposed that the microscopic field correction factor L for the Raman-scattering cross sections for liquids is

$$L = \frac{[\epsilon(\omega_s) + 2]^2 [\epsilon(\omega_{\text{in}}) + 2]^2}{81} . \quad (32)$$

Since Raman scattering involves both absorption and emission processes, the correction factor L is a product of the microscopic field correction factors for both absorption and emission. There is general agreement that Eq. (32) adequately describes the microscopic field effect on Raman-scattering cross sections of liquids.¹⁸ Since the refractive indices of liquid nitrobenzene at 4880 and at 5223 Å are 1.57 and 1.56, respectively, the correction factor L is 4.84. The cross section for liquid nitrobenzene is 6.68 times that of gaseous nitrobenzene. Thus, we see that the cross section increase in going from gas to liquid phase is mainly due to the microscopic field effect. The remaining small factor of 1.38 may be attributed to the effect of intermolecular interactions. For benzene the cross section for the liquid is 3.27 times greater than that for the gas. The microscopic field correction factor L for liquid benzene is expected to be 3.81 based on the refractive index at 4880 and 5128 Å of 1.48. Thus, for benzene the cross section change between gas and liquid is totally due to the microscopic field effect.

In going from the liquid phase to the amorphous

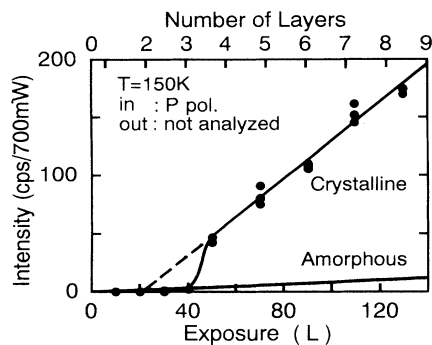


FIG. 12. Raman intensity of the NO_2 symmetric stretching mode from a crystalline nitrobenzene layer on Ni(111) at 150 K as a function of exposure (Ref. 2). The incident power was 700 mW at the sample and the wavelength was 4880 Å. The incident and scattered angles were 60° and 32° , respectively. The incident light was p polarized and the scattered light was not analyzed. The spectrometer resolution was set at 24 cm^{-1} , and the effective solid angle of collection was 0.0284 sr . The solid curve labeled "amorphous" is the calculated Raman intensity of the amorphous nitrobenzene layer for the same scattering geometry. This curve is based on the Raman cross section and depolarization ratio obtained in the present work.

phase, the dielectric constant of nitrobenzene does not change significantly. Thus, there is little change in the microscopic field correction factor L . On the other hand, the Raman cross section changes by more than a factor of 4. This change must be explained by intermolecular interactions. Of course, when the intermolecular interaction is very strong, we are no longer justified in viewing the cross section in molecular terms. Instead, we should consider it to be a new property of the condensed phase. Indeed, when the amorphous layer crystallizes there is an even greater change in the Raman cross section.

Figure 12 taken from our previous work² shows the Raman intensity from the adsorbed layer of nitrobenzene as a function of coverage below nine monolayers. Below three monolayers the layer is amorphous and there is a single Raman peak as shown in Fig. 8. The peak splits into two peaks above three monolayers, and the Raman intensity suddenly increases. This transition around three monolayers is interpreted as corresponding to the start of crystallization. The Raman intensity of an amorphous nitrobenzene layer calculated from the cross sec-

tion and depolarization ratio determined in the present work is also plotted in Fig. 12 where it is denoted by "amorphous." The observed difference between the amorphous and crystalline phases is clearly due to the difference in the intermolecular interactions. When the layer crystallizes, the molecular vibrations of neighboring molecules interact so strongly that they split into two factor groups and become the optical phonons of the crystalline structure. Thus, in this limit of strong intermolecular interaction the molecular vibrations as such cease to exist. In this limit it is no longer meaningful to compare the Raman cross sections of different phases.

VII. CONCLUSION

We have determined the absolute Raman-scattering cross section of an amorphous nitrobenzene layer on Ni(111). Since the optical effect of the substrate was separated out by using the electromagnetic Green's function, the cross section obtained here is a property of the sample system (adsorbate layer) independent of the optical environment in which it is placed. We have also measured the absolute cross sections for gaseous and liquid nitrobenzene. The ratios of the cross sections in the three different states are gas:liquid:amorphous=1:7:29. We found that the cross section of a crystalline nitrobenzene layer on Ni(111) is much larger than that of the amorphous layer. The cross-section change on going from gaseous to liquid nitrobenzene is mainly due to the microscopic field effect and partially due to intermolecular interactions. On the other hand, the cross-section change on going from the liquid to an amorphous layer, and from an amorphous layer to a crystalline layer, is mainly due to intermolecular interactions.

ACKNOWLEDGMENTS

We would like to thank Professor K. Ueda for lending us a standard halogen lamp, and Professor T. Nagata at Tokyo University for the data on the vapor pressure of nitrobenzene near room temperature. We also thank Professor J. M. Lawrence of the University of California, Irvine, for helpful comments on the manuscript. This paper was completed while one of us (S.U.) was on a sabbatical leave at the University of California, Irvine. He wishes to thank the Physics Department and Professor D. L. Mills for the hospitality. This work was supported in part by a Grant-in-Aid for Scientific Research from the Ministry of Education, Science and Culture.

*Present address: Japan Advanced Institute of Science and Technology, Tatsunokuchi-machi, Nomi-gun, Ishikawa-ken 923-12, Japan.

¹K. Sakamoto, G. Mizutani, Y. Kondo, and S. Ushioda, *Surf. Sci.* **221**, 61 (1989).

²K. Sakamoto, G. Mizutani, and S. Ushioda, *Surf. Sci.* **259**, 79 (1991).

³Y. Kondo, G. Mizutani, K. Sakamoto, and S. Ushioda, *Mater. Sci. Eng. B* **7**, 177 (1990).

⁴M. Kuwahara, G. Mizutani, K. Sakamoto, and S. Ushioda,

Surf. Sci. **242**, 544 (1990).

⁵C. E. Reed, J. Giergiel, J. C. Hemminger, and S. Ushioda, *Phys. Rev. B* **36**, 4990 (1987). We note that the definition of the angles θ_{in} and θ_s in the present paper is different from that defined by Reed *et al.* One must replace θ as defined by Reed *et al.* by $(\pi/2 - \theta_{in})$ or $(\pi/2 - \theta_s)$ for the present definition.

⁶J. Giergiel, C. E. Reed, J. C. Hemminger, and S. Ushioda, *J. Phys. Chem.* **92**, 5357 (1988).

⁷E. B. Wilson, Jr., J. C. Decius, and P. C. Cross, *Molecular Vi-*

- brations* (Dover, New York, 1980), pp. 285–286.
- ⁸H. Sano, G. Mizutani, and S. Ushioda, *Surf. Sci.* **223**, 621 (1989).
- ⁹A. A. Maradudin and D. L. Mills, *Phys. Rev. B* **11**, 1392 (1975).
- ¹⁰D. L. Mills and A. A. Maradudin, *Phys. Rev. B* **12**, 2943 (1975).
- ¹¹D. A. Long, *Raman Spectroscopy* (McGraw-Hill, New York, 1977), pp. 43–48.
- ¹²J. G. Skinner, and W. G. Nilsen, *J. Opt. Soc. Am.* **58**, 113 (1968).
- ¹³Y. Kato and H. Takuma, *J. Opt. Soc. Am.* **61**, 347 (1971).
- ¹⁴M. Trenary, K. J. Uram, F. Bozso, and J. T. Yates, Jr., *Surf. Sci.* **146**, 269 (1984).
- ¹⁵P. B. Johnson and R. W. Christy, *Phys. Rev. B* **12**, 5056 (1974).
- ¹⁶K. Kurosawa, R. M. Pierce, S. Ushioda, and J. C. Hemminger, *Phys. Rev. B* **33**, 789 (1986).
- ¹⁷H. W. Schrötter and H. J. Bernstein, *J. Mol. Spectrosc.* **12**, 1 (1964).
- ¹⁸H. W. Schrötter and H. W. Klöckner, in *Raman Spectroscopy of Gases and Liquids*, edited by A. Weber (Springer-Verlag, Berlin, 1979), pp. 123–166.
- ¹⁹T. Fujiyama, *J. Raman Spectrosc.* **12**, 199 (1982).
- ²⁰G. Eckhardt and W. G. Wagner, *J. Mol. Spectrosc.* **19**, 407 (1966).